MESHLESS LOCAL PETROV-GALERKIN METHOD FOR 2 DIMENSIONAL ELASTICITY PROBLEMS

Pamuda PUDJISURYADI[1], Effendy TANOJO[1]

ABSTRACT: Meshless methods are alternative solutions in response to Finite Element Method's drawbacks such as locking problem, element distorsion, and effort of remeshing. Redescritization in meshless methods can be done by simply adding nodes in regions where the accuracy of the solutions need to be improved. In this study, one of the meshless methods called the Meshless Local Petrov-Galerkin (MLPG) is introduced. The accuracy of the method which is using the Moving Least-Squares (MLS) approximation is demonstrated. A standard cantilever beam with end tip point load problem is analysed by MLPG as well as finite element method (SAP2000) for comparison. Numerical results show that analysis using the MLPG is satisfactory.

KEYWORDS: Meshless Local Petrov-Galerkin, Moving Least-Squares.

1. INTRODUCTION

Finite Element Method (FEM) is one of well established numerical solutions for engineering problems. Some drawbacks of FEM are locking problems, element distortions, and remeshing for large displacement problems [1-2]. In recent years, meshless methods have been developed as alternative numerical approaches in efforts to eliminate known drawbacks of the FEM. The main objective to these methods is to reduce the difficulty of meshing and remeshing of complex structural problem domains. Descritization procedure of the problem domain is done only by simply adding or deleting nodes where desired. Nodal connectivity to form an element as in FEM is not needed, only nodal coordinates and their Domain of Influence (DOI) are necessary to descretize the problem domain.

There are several meshless methods under current development, including the Element-Free Galerkin (EFG) method proposed by Belytschko et al. [3], the Reproducing Kernel Particle Method (RKPM) proposed by Liu et al. [4], Smooth Particle Hydrodynamics (SPH) method proposed by Gingold and Monaghan [5], Meshless Local Petrov-Galerkin (MLPG) method proposed by Atluri et al. [1], and some other methods. The newly developed MLPG method use shape functions which are derived from moving least-square (MLS) approximation. The main purpose of this paper is to compare the accuray of MLPG compared to exact solution and FEM method (SAP2000) in a standard cantilever beam problem [6].

2. MOVING LEAST-SQUARES (MLS) APPROXIMATION

Given a set of nodes $\mathbf{x}_I$ and a set of nodal values u_I the original function f:$f(\mathbf{x}_i)= u_i$ is to be approximated using no connectivity information. Consider the approximation as a product of polynomial basis function and a set of coefficients as follows:

[1] *Lecturer, Dept. of Civil Engineering, Petra Christian University, Indonesia.*

$$u_{app}(\mathbf{x}) = \mathbf{p}^T(\mathbf{x}) \quad \mathbf{a}(\mathbf{x}) = \sum_{j=1}^{m} p_j(\mathbf{x}) \quad a_j(\mathbf{x}) \tag{1}$$

where **p,** the polynomial basis function, is a vector with the size *m*x1 (*m* is the number of polynomial coefficients), and **a** is a set of coefficients. Examples of polynomial bases and coefficients **a** are presented in Table 1.

Table 1. Polynomial bases

1D	$\mathbf{p}^T = [1, x, x^2, \ldots, x^n]$
2D	$\mathbf{p}^T = [1, x, y, \ldots x^n, y^n]$
3D	$\mathbf{p}^T = [1, x, y, z, \ldots, x^n, y^n, z^n]$
	$\mathbf{a}^T = [a_1, a_2, \ldots, a_m]$

It should be noted here that the coefficients used in the approximation (**a**) depend on the location where the original function is approximated, this is different from the approximation coefficients used in FEM which are constant. Determination of **a** is achieved by minimizing a weighted square of discrete error of the function *u* expressed in following term :

$$J = \sum_{I=1}^{N} w_I(\mathbf{x} - \mathbf{x}_I)[u_{app}(\mathbf{x}_I, \mathbf{x}) - u_I]^2 \tag{2}$$

where $w_I(x - x_I)$ is the degree of influence (weight function) of node *I* to a point **x** in the problem domain and $u_{app}(\mathbf{x}_I, \mathbf{x}) = \mathbf{p}^T(\mathbf{x}_I)\mathbf{a}(\mathbf{x})$. Weight function of a point *I* has a unit value at that point and smoothly decrease as we move further from that point and finally reach zero value at a certain distance (radius) d_{max}. In matrix form, Equation 2 can be rewritten as:

$$J = (\mathbf{Pa} - \mathbf{u})^T \mathbf{W}(\mathbf{Pa} - \mathbf{u}) \tag{3}$$

where

$$\mathbf{u}^T = (u_1, u_2, \ldots, u_N)$$

$$\mathbf{P} = \begin{bmatrix} p_1(\mathbf{x}_1) & p_2(\mathbf{x}_1) & \ldots & p_m(\mathbf{x}_1) \\ p_1(\mathbf{x}_2) & p_2(\mathbf{x}_2) & \ldots & p_m(\mathbf{x}_2) \\ \vdots & \vdots & & \vdots \\ p_1(\mathbf{x}_N) & p_2(\mathbf{x}_N) & \ldots & p_m(\mathbf{x}_N) \end{bmatrix}$$

$$\mathbf{W}(\mathbf{x}) = \begin{bmatrix} w_1(\mathbf{x}-\mathbf{x}_1) & 0 & \ldots & 0 \\ 0 & w_2(\mathbf{x}-\mathbf{x}_2) & & \vdots \\ \vdots & & \ddots & \vdots \\ 0 & \ldots & 0 & w_N(\mathbf{x}-\mathbf{x}_N) \end{bmatrix}$$

The coefficients **a** can be determined by minimizing Equation 3 with the respect to coefficients **a** which lead to following expression :

$$\mathbf{a}(\mathbf{x}) = \mathbf{A}^{-1}(\mathbf{x})\mathbf{B}(\mathbf{x})\mathbf{u} \tag{4}$$

where

$$\mathbf{A}(\mathbf{x}) = \mathbf{P}^T\mathbf{W}(\mathbf{x})\mathbf{P}$$
$$\mathbf{B}(\mathbf{x}) = \mathbf{P}^T\mathbf{W}(\mathbf{x})$$

Then the approximation of the original function in Equation 1 can be obtained. Substituting Equation 4 into Equation 1 and rearrange the equation according to nodal value u_I, Equation 1 can be rewritten in this form:

$$u_{app}(\mathbf{x}) = \sum_{I=1}^{N} \Phi_I(\mathbf{x}) u_I \tag{5}$$

where $\Phi_I(\mathbf{x}) = \mathbf{p}^T(\mathbf{x})\mathbf{A}^{-1}(\mathbf{x})\mathbf{B}_I(\mathbf{x})$ is known as the MLS shape function of node *I*. $\mathbf{B}_I(\mathbf{x})$ is the I^{th} column of matrix $\mathbf{B}(\mathbf{x})$. These following equations are formulation to determine the shape functions derivatives:

$$\begin{aligned}\Phi_{I,\mathbf{x}} &= (\mathbf{p}^T\mathbf{A}^{-1}\mathbf{B}_I)_{,\mathbf{x}} \\ &= \mathbf{p}^T{}_{,\mathbf{x}}\mathbf{A}^{-1}\mathbf{B}_I + \mathbf{p}^T(\mathbf{A}^{-1})_{,\mathbf{x}}\mathbf{B}_I + \mathbf{p}^T\mathbf{A}^{-1}\mathbf{B}_{I,\mathbf{x}}\end{aligned} \tag{6}$$

where

$$\mathbf{B}_{I,\mathbf{x}}(\mathbf{x}) = \frac{dw}{d\mathbf{x}}(\mathbf{x}-\mathbf{x}_I)\mathbf{p}(\mathbf{x}_I),$$
$$\mathbf{A}^{-1}{}_{,\mathbf{x}} = -\mathbf{A}^{-1}\mathbf{A}_{,\mathbf{x}}\mathbf{A}^{-1},$$
$$\mathbf{A}_{,\mathbf{x}} = \sum_{I=1}^{n} \frac{dw}{d\mathbf{x}}(\mathbf{x}-\mathbf{x}_I)\mathbf{p}(\mathbf{x}_I)\mathbf{p}^T(\mathbf{x}_I).$$

3. MESHLESS LOCAL PETROV-GALERKIN (MLPG) METHOD

For a two-dimensional linear, elastic boundary value problem in a global domain Ω, bounded by Γ (Figure 1), the force equilibrium equation can be written as:

$$\sigma_{ij,j} + b_i = 0 \quad in\ \Omega \tag{7}$$

where σ_{ij} is the stress tensor, b_i are the body forces, and $\sigma_{ij,j}$ indicates the partial derivative of σ_{ij} with respect to coordinate direction x_j. Additionally, the boundary conditions may be written, respectively, as:

$$u_i = \bar{u}_i \qquad at\ \Gamma_u \tag{8}$$

$$\sigma_{ij}n_j = \bar{t}_i \quad at\ \Gamma_t \tag{9}$$

where u_i is i^{th} component of displacement, $\overline{u}_i$ and $\overline{t}_i$ are prescribed displacements and tractions that are applied on boundary segments Γ_u and Γ_t, respectively, and n_j is the unit vector that is locally outward normal to the boundary. A generalized local weak form of the governing differential equation and the boundary conditions, over a local sub-domain $\Omega_{te}^I \in \Omega$, as shown in Figure 1, can be written as [1]:

$$\int_{\Omega_{te}^I} \left(\sigma_{ij,j} + b_i\right) v_i \, d\Omega - \alpha \int_{\Gamma_{su}^I} \left(u_i - \overline{u}_i\right) v_i \, d\Gamma = 0 \tag{10}$$

where Γ_{su}^I is the intersection of Γ_u and the boundary $\partial\Omega_{te}^I$ of Ω_{te}^I, v_i is a test function that can be chosen with some degree of flexibility, and α is a penalty parameter that sets the degree of influence of the second term in (10) with respect to the first term. The definitions of the various regions and boundaries relevant to the formulation of the MLPG method are clearly illustrated in Figure 2.

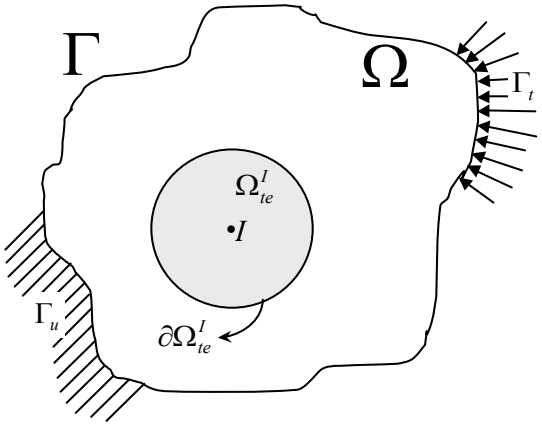

Figure 1. A schematic representation of the sub-domain Ω_{te}^I, with node *I* as its center.

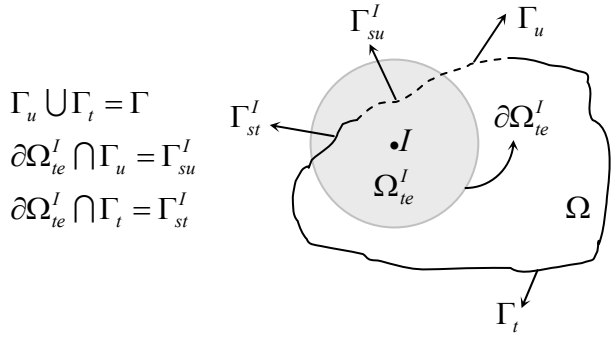

Figure. 2. Definitions if the domain of the test function Ω_{te}^I intersects the global boundary Γ.

Further, if integration by parts and the divergence theorem are applied to the first term of Equation 10, the equation can be expressed as follows:

$$\int_{\partial\Omega_{te}^I} \sigma_{ij} n_j v_i d\Gamma - \int_{\Omega_{te}^I} \sigma_{ij} v_{i,j} d\Omega + \int_{\Omega_{te}^I} b_i v_i d\Omega - \alpha \int_{\Gamma_{su}^I} (u_i - \overline{u}_i) v_i d\Gamma = 0 \tag{12}$$

Noting that test function $v_i = 0$ on $\partial\Omega_{te}^I$ except if $\partial\Omega_{te}^I$ intersects a global boundary Γ, Equation 11 can be rewritten as:

$$\int_{\Gamma_{su}^I} \sigma_{ij} n_j v_i d\Gamma + \int_{\Gamma_{st}^I} \sigma_{ij} n_j v_i d\Gamma - \int_{\Omega_{te}^I} \sigma_{ij} v_{i,J} d\Omega + \int_{\Omega_{te}^I} b_i v_i d\Omega - \alpha \int_{\Gamma_{su}^I} (u_i - \bar{u}_i) v_i d\Gamma = 0 \qquad (12)$$

Finally, Equation 12 can be re-written in the following form (known as the local symmetric weak form):

$$\int_{\Omega_{te}^I} \sigma_{ij} v_{i,J} d\Omega + \alpha \int_{\Gamma_{su}^I} u_i v_i d\Gamma - \int_{\Gamma_{su}^I} t_i v_i d\Gamma = \int_{\Gamma_{st}^I} \bar{t}_i v_i d\Gamma + \alpha \int_{\Gamma_{su}^I} \bar{u}_i v_i d\Gamma + \int_{\Omega_{te}^I} b_i v_i d\Omega \qquad (13)$$

where Γ_{st}^I is the intersection of Γ_t and the boundary $\partial\Omega_{te}^I$, and $t_i = \sigma_{ij} n_j$. Equation 13 leads to the I^{th} row of the global stiffness matrix. The J^{th} columns of the stiffness matrix correspond to all nodes whose domains of influence Ω_{tr}^J intersect with the I^{th} test function's sub-domain Ω_{te}^I, as shown in Figure 3.

Further, it can be shown if the radius of Ω_{tr}^J and Ω_{te}^I for each I and J are equal, and if u_i and v_i centered at the I^{th} and J^{th} nodes, respectively, are the same for each I and J, then the stiffness matrix will be symmetric. In this study, the test function v_i is equal to zero at $\partial\Omega_{te}^I$ except if $\partial\Omega_{te}^I$ intersects the global boundary Γ, and the test function v_i is any function that is sufficiently well-behaved and integrable [7]. This means that the test function can take any shapes such as circular, ellipse, rectangular, polygonal, etc., as long as the above criterions are met.

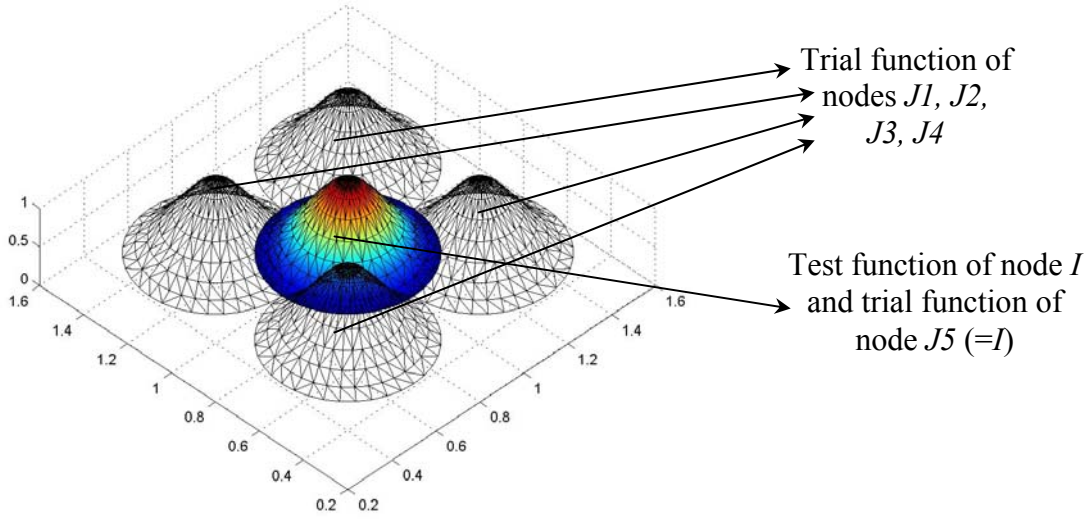

Figure 3. Intersections of test function and trial functions which lead to non-zero components in the I^{th} row of stiffness matrix.

To obtain the discrete equations from the MLPG formulation (13), the trial function u_i and test function v_i are defined as follows:

$$u_i(x) = \sum_{J=1}^{N} \phi^J(x) \hat{u}_i^J \text{ , and} \qquad (14a)$$

$$v_i(x) = \sum_{I=1}^{N} \psi^I(x)\hat{v}_i^I \tag{14b}$$

where $\phi^J(x)$ and $\psi^I(x)$ are the nodal shape functions for the trial and test functions, respectively, and are centered at nodes J and I, respectively. The $\phi^J(x)$ are constructed from Moving Least-Square (MLS) approximation functions and the $\psi^I(x)$ are chosen as the weight functions used in MLS approximation at node I. Thus each nodal sub-domain is circular in shape. In typical meshless interpolations, $\hat{u}_i^J$ are referred to fictitious nodal values since they have no real physical meaning. Due to the nature of MLS approximation functions, which are not necessarily equal to unity at its corresponding node and equal to zero at their neighboring nodes, the nodal degrees of freedom in MLS based methods do not correspond to actual displacements at the nodes.

Substituting Equation 14 into Equation 13 and factoring $\hat{v}_i^I$ out of the equation, the discrete form of the MLPG formulation can be expressed as follows:

$$\begin{aligned}\sum_{J=1}^{N}\int_{\Omega_{te}^I}\left(B_v^I\right)^T DB^J\hat{u}^J d\Omega + \alpha\sum_{J=1}^{N}\int_{\Gamma_{su}^I} V^I\phi^J\hat{u}^J d\Gamma - \sum_{J=1}^{N}\int_{\Gamma_{su}^I} V^I NDB^J\hat{u}^J d\Gamma \\ = \int_{\Gamma_{st}^I} V^I\bar{t}\,d\Gamma + \alpha\int_{\Gamma_{su}^I} V^I\bar{u}\,d\Gamma + \int_{\Omega_{te}^I} V^I b\,d\Omega\end{aligned} \tag{15}$$

where in two-dimensional space,

$$B_v^I = \begin{bmatrix}\psi_{,1}^I & 0\\ 0 & \psi_{,2}^I\\ \psi_{,2}^I & \psi_{,1}^I\end{bmatrix},\ B^J = \begin{bmatrix}\phi_{,1}^J & 0\\ 0 & \phi_{,2}^J\\ \phi_{,2}^J & \phi_{,1}^J\end{bmatrix},\ N = \begin{bmatrix}n_1 & 0 & n_2\\ 0 & n_2 & n_1\end{bmatrix}$$

$$V^I = \begin{bmatrix}\psi^I & 0\\ 0 & \psi^I\end{bmatrix},\ \hat{u}^J = \begin{Bmatrix}\hat{u}_1^J\\ \hat{u}_2^J\end{Bmatrix},\ D = \frac{\bar{E}}{1-\bar{\upsilon}^2}\begin{bmatrix}1 & \bar{\upsilon} & 0\\ \bar{\upsilon} & 1 & 0\\ 0 & 0 & \dfrac{1-\bar{\upsilon}}{2}\end{bmatrix}$$

and

$$\bar{E} = \begin{cases} E \\ E/(1-\upsilon^2)\end{cases} \text{ and } \bar{\upsilon} = \begin{cases} \upsilon & \text{for plane stress}\\ \upsilon/(1-\upsilon) & \text{for plane strain}\end{cases}.$$

Further, Equation 15 can be written in a more compact form which we may already be familiar with, namely:

$$\sum_{J=1}^{N} K_{IJ}\hat{u}^J = f_I \tag{16}$$

where

$$\begin{aligned}K_{IJ} &= \int_{\Omega_{te}^I}\left(B_v^I\right)^T DB^J d\Omega + \alpha\int_{\Gamma_{su}^I} V^I\phi^J d\Gamma - \int_{\Gamma_{su}^I} V^I NDB^J d\Gamma\\ f_I &= \int_{\Gamma_{st}^I} V^I\bar{t}\,d\Gamma + \alpha\int_{\Gamma_{su}^I} V^I\bar{u}\,d\Gamma + \int_{\Omega_{te}^I} V^I b\,d\Omega\end{aligned}. \tag{17}$$

In the MLPG method, each local weak form (examining only one test function and the trial functions whose domains intersect with its domain) results in two rows (for two dimensional problems) of non-zero components of the global stiffness matrix. Theoretically, as long as the union of all local sub-domains Ω_{te}^{I} covers the global domain, the equilibrium equation and the boundary conditions will be satisfied in the entire global domain Ω and along its boundary Γ [1]. Solving Equation 16, the fictitious nodal displacement values $\hat{u}^{J}$ at every node J can be obtained. Approximate solution can be obtained from Equation 14a, and by taking the derivative of this approximate solution and applying an appropriate stress-strain relationship (the Hooke's Law), the strain and the stress can be obtained.

4. CANTILEVER BEAM PROBLEM

A standard cantilever beam test (loaded at its free end) as can be seen in Figure 4, will be analyzed.

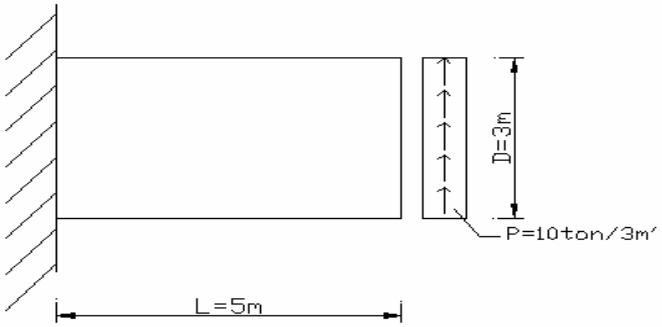

Figure 4. Cantilever beam test

The exact displacement solutions are given in Equations 19, and 20 [6] as follows :

$$\bar{u}_1 = \frac{-P}{6\ E\ IM}\left(y-\frac{D}{2}\right)\left(3x(2L-x)+(2+\upsilon)y(y-D)\right) \tag{18}$$

$$\bar{u}_2 = \frac{P}{6\ E\ IM}\left(x^2(3L-x)+3\upsilon(L-x)\left(y-\frac{D}{2}\right)^2+(4+5\upsilon)D^2\frac{x}{4}\right) \tag{19}$$

where $\bar{u}_1$ = horizontal displacement

$\bar{u}_2$ = vertical displacement

IM = Second moment of Inertia

υ = poisson's ratio

The cantilever beam is analyzed with 7x11 nodal configuration using MLPG (linear, bilinear, quadratic, cubic polynomials) and FEM (SAP2000, 4 noded bilinear element). Displacement results are observed in midspan section of the beam, as can be seen in these following figures.

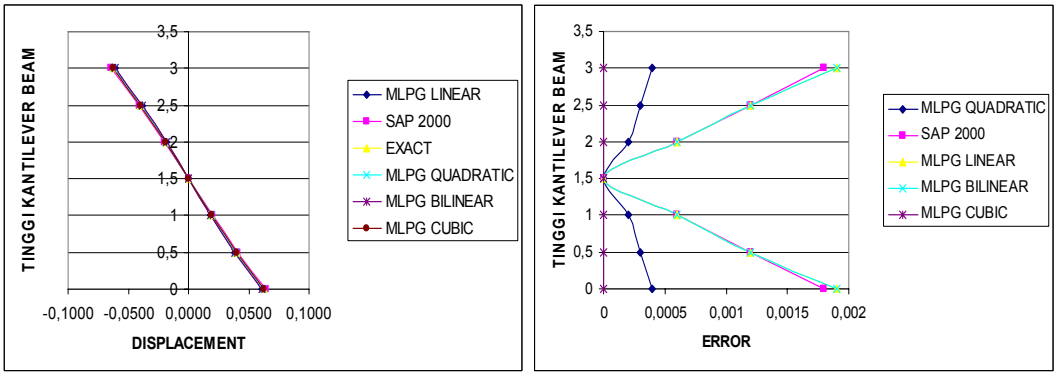

Figure 5. Displacement and displacement error in X direction at midspan [8].

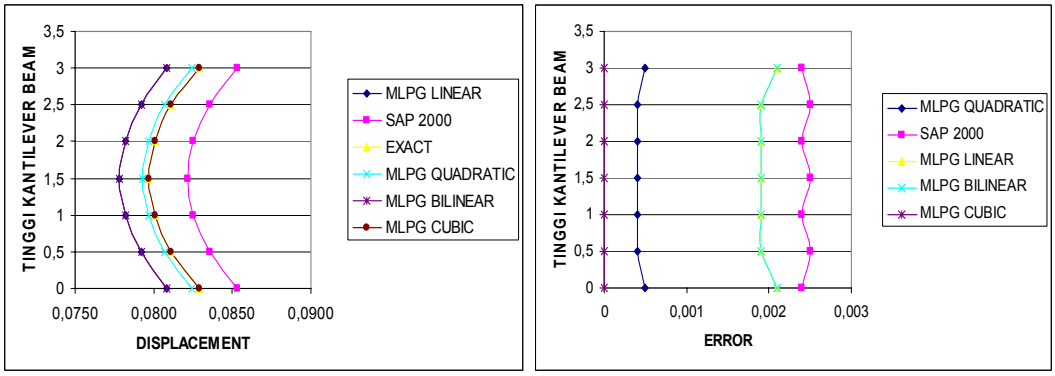

Figure 6. Displacement and displacement error in Y direction at midspan [8].

5. CONCLUSIONS

From the cantilever beam test, some points can be concluded.

1. In MLPG, value of *error displacement* is lower if higher polynomial function is used.
2. With the same number of nodes and the same polynomial function (bilinear), MLPG results show better error displacement than FEM results (SAP2000).
3. MLPG approaches the exact solution from risky side (underestimates the displacement), while FEM (SAP2000) approaches the exact solution from conservative side (overestimates the displacement).

6. REFERENCES

1. Atluri, S.N. and Zhu, T. "A New Meshless Local Petrov-Galerkin (MLPG) Approach in Computational Mechanics." *Computational Mechanics* 22 (1998): 117-127.
2. Atluri, S.N., Kim, H.-G. and Cho, J.Y. "A Critical Assessment of The Truly Meshless Local Petrov-Galerkin (MLPG), and Local Boundary Integral Equation (LBIE) Methods." *Computational Mechanics* 24 (1999): 348-372.
3. Belytschko, T., Lu, Y.Y., Gu, L., 1994. Element-free Galerkin methods. *International Journal for Numerical Methods in Engineering* 37: 229-256.
4. Liu, W.K., Jun, S., Zhang, Y.F., 1995. Reproducing kernel particle methods. *International Journal for Numerical Methods in Fluids* 20: 1081-1106.
5. Gingold, R.A., Monaghan, J.J., 1977. Smoothed particle hydrodynamics: theory and application to non-spherical stars. *Mon. Not. Roy. Astron. Soc*. 181: 375-389.
6. Timoshenko and Goodier "*Theory of Elasticity*." McGraw-Hill Book Company, New York. 1970.
7. Becker, E.B., Carey, G.F., Oden, J.T. *Finite Element: An Introduction*, Volume I, New Jersey: Prentice-Hall, Inc., 1981.
8. Yulianti, Junaidi, B., Pudjisuryadi, P., Tanojo, E. "Aplikasi Meshless Local Petrov-Galerkin pada Analisis Problem Elastisitas Struktural Dua Dimensi." *PETRA Christian University Thesis*, Surabaya, 2004.